RSC Advances

PAPER

View Article Online
View Journal | View Issue

Cite this: *RSC Adv.*, 2024, **14**, 15232

Rapid catalytic reduction of environmentally toxic azo dye pollutant by Prussian blue analogue nanocatalyst†

Dina A. El Mously, [a] Amr M. Mahmoud, *[a] Mohammed M. Gomaa [b] and Hend Z. Yamani *[c]

The release of toxic azo dyes pollutants in the environment from different industries represents a public health concern and a serious environmental problem. Therefore, the conversion of hazardous methyl orange (MO) azo dye to environmentally benign products is a critical demand. In this work, an eco-friendly Prussian blue analogue (PBA) was synthesized and its catalytic activity toward the reduction of MO was investigated. The PBA copper(II) hexacyanocobaltate(III) ($Cu_3[Co(CN)_6]_2$) was synthesized by a facile inexpensive chemical coprecipitation method without using hazardous solvents. The nanocatalyst was characterized using XPS, Raman, FTIR spectroscopy, and XRD. The chemical reduction of MO using $NaBH_4$ and the PBA as nanocatalyst was monitored by UV-VIS spectroscopy. Toxic MO was completely reduced in 105 s with a rate constant (k) 0.0386 s^{-1} using only 10 μg of the PBA nanocatalyst. Besides the powerful catalytic activity, the nanocatalyst also showed excellent stability and recyclability for ten consecutive cycles, with no significant decrease in the catalytic performance. Therefore, the proposed PBA is a promising, stable, cost-effective, and eco-friendly nanocatalyst for the rapid elimination of hazardous azo dyes.

Received 15th November 2023
Accepted 20th April 2024

DOI: 10.1039/d3ra07806j

rsc.li/rsc-advances

Introduction

Synthetic azo dyes are used in various industries such as textile dyeing, leather tanning, paper, paint, and cosmetics processing. Azo dyes represent nearly two thirds of all synthetic dyes and considered the most widely used class of dyes in industries. These industries discharge millions of gallons of toxic hazardous wastes containing synthetic dyes into the environment.[1] The untreated dyes effluents represent a major public health concern and a serious environmental problem. Many azo dyes as MO were proved to be carcinogenic, mutagenic, and genotoxic to human and as well as animals.[2] A thin film of discharged dyes is formed over the water surface leading to reduction of sunlight penetration and dissolved oxygen. Accordingly, this impairs the aquatic plants photosynthetic activity. The toxic effluent may be lethal to certain forms of marine life. Moreover, seed germination process and soil quality are negatively affected if the effluent finds its way to agricultural land.[3] Therefore, their removal from industrial effluent is crucial. Environmental agencies guidelines state that industrial effluents must be treated before being discharged into water resources.

Azo dyes are highly water soluble, stable in light and, resistant to biodegradation.[4] Accordingly, conventional treatment methods are frequently ineffective. Therefore, there is a prime need to develop eco-friendly and cost-effective approaches for treatment of dye containing effluent prior to its discharge into the environment.[5] Different methods were reported for either removal or breaking down toxic azo dyes into harmless products. Physical methods such as flocculation,[6] membrane filtration, adsorption,[7] and ion exchange[8] were used in the removal of dyes. However, physical methods just transfer the dyes to another phase instead of destroying them.[9] Their application has been restricted due to their low decolorization efficacy, generation of large amount of sludge, high cost of some adsorbents and membranes, and possible membrane fouling.[4] Biodegradation using enzymes or different microorganisms as bacteria, fungi, yeast, and algae to eliminate dyes in textile effluent was reported. The disadvantages of this approach are the low degradation efficiency and long operation time.[10] The electrochemical treatment of dye containing effluent as anodic oxidation, electro-Fenton, and electrocoagulation suffer from certain drawbacks as the high cost of electricity, possibility of electrodes fouling, and being less effective than other treatment technologies.[5]

[a]*Pharmaceutical Analytical Chemistry Department, Faculty of Pharmacy, Cairo University, Cairo 11562, Egypt. E-mail: dina.abbas@pharma.cu.edu.eg*
[b]*Solid State Physics Department, National Research Centre, Giza 12622, Egypt*
[c]*Pharmaceutical Analytical Chemistry Department, Faculty of Pharmacy, Ain Shams University, Cairo 11566, Egypt*

† Electronic supplementary information (ESI) available. See DOI: https://doi.org/10.1039/d3ra07806j

On the other hand, catalytic reduction of azo dyes containing effluent using $NaBH_4$ as reducing agent is simple, time saving, with high conversion rates. Furthermore, there is no need for expensive working setups, energy source, or potential window selection. Reduction of MO with $NaBH_4$ is thermodynamically feasible. However, the large kinetic barrier between the MO as electron acceptor and $NaBH_4$ as electron donor make the reaction kinetically difficult. Thus, the uncatalyzed reaction is tremendously slow, even in presence of large amount of $NaBH_4$. Catalysts can make the reaction kinetically favorable by reducing the activation energy, and accordingly decreasing kinetic barrier.[11,12] Therefore, a stable, cost-effective, and eco-friendly catalyst is needed to facilitate the transfer of electrons between MO with $NaBH_4$.

Over the last years, the use of nanocatalysts in the reduction of MO has devoted much attention. Nanocatalysts provide faster reaction rates compared to ordinary catalysts. This may be attributed to the larger surface area for electron transfer offered by smaller particle size. Different nanocatalysts were reported in the literature for catalytic reduction of MO including metal nanoparticles as Ag NPs,[13,14] Pd NPs,[15] and Cu NPs[16] or nanocomposites as CuAg/ZnO/carbon black-cellulose acetate sheets,[17] PANI/NiO,[18] $NiFe_2O_4/\gamma$-Fe_2O_3, $CoFe_2O_4/\gamma$-Fe_2O_3,[19] and C@Fe.[20] Although they exhibit good catalytic activity, the need for more affordable and effective nanocatalysts has driven more research in this field.

Prussian blue analogues (PBAs) are a large family of metal–organic framework materials with an open framework structure. This large PBAs family has been widely explored in various fields due to their interesting open framework, porosity, tunable channels, redox chemistry, high surface area, controllable size, tunable morphology, high charge transfer, photomagnetic characteristics, simple and low-cost preparation. Due to their exceptional properties, PBAs have found a broad application range in energy storage and conversion,[21] catalysis, electrochemical sensors, and biosensors.[22] Moreover, PBAs nanoparticles are characterized by biosafety, biocompatibility, and biodegradability making them attractive candidates in biomedicine applications as drug carriers, nanoenzymes, imaging agents, and antidote for radioactive contamination with thallium and caesium. Their application in phototherapy lay on their good photostability and high photothermal conversion efficiency.[23]

The tunable physicochemical properties and remarkable diversity make PBAs suitable and attractive materials for environmental purification and decontamination. Some of the most common applications are removing toxic ions from aqueous media, water desalination, air decontamination, and degradation of hazardous pollutants.[24,25]

The PBAs are cyanide complexes with the chemical formula $A_xT[M(CN)_6]\cdot nH_2O$, where A represents an alkaline ion (Li, Na, K), T represents external transition metal (T = Cu, Co, Fe, Mn, Zn, Ni, Cd, *etc.*), and M resembles internal transition metal (M = Fe, Co, Cr, Mn, Ru, Os, Rh, Ir, Pd).[24] Due to the abundant transition metal in the framework, PBAs and their derivatives can be applied as catalysts.[26] The various possible A, T, and M metal combinations result in remarkable diversity in the PBA family with tunable catalytic activity.[27] The synergetic effect among transition metals, those catalytic systems bearing this property could enhance the catalytic activity compared to the single metal-based ones.[28] Among the various transition metals, copper and cobalt are well known for their effective catalytic activity.[27,29–31]

Moreover, one of the main advantages of PBAs based catalysts is their simple inexpensive preparation. Compared to materials with similar structural features, such as MOFs, PBA has the advantage of having higher stability in water under a wide pH range.[25] They are characterized with powerful catalytic activity in degradation process of pollutants compared to different catalysts reported in the literature.[13,14,18,19]

Accordingly, in this work, the PBA; copper(II) hexacyanocobaltate(III) ($Cu_3[Co(CN)_6]_2$) nanoparticle were synthesized by a facile inexpensive chemical coprecipitation and investigated as nanocatalyst for the catalytic reduction of toxic MO azo dye.

Experimental

Chemicals and reagents

Sodium borohydride ($NaBH_4$), methyl orange (MO), potassium hexacyanocobalate(III) $K_3[Co(CN)_6]$, and copper sulfate pentahydrate ($CuSO_4\cdot 5H_2O$), were purchased from Sigma-Aldrich (Germany). Acetic acid, boric acid, phosphoric acid, and sodium hydroxide for Britton Robinson buffer (BRB) preparation were obtained from Piochem (Egypt).

Synthesis of PBA $Cu_3[Co(CN)_6]_2$

The PBA was synthesized by co-precipitated method as reported in the literature[32] with some modification. Briefly, 100 mL of $K_3[Co(CN)_6]$ (0.05 M) was heated to 80 °C, then 150 mL of $CuSO_4\cdot 5H_2O$ (0.05 M) was added drop-wise under magnetic stirring and the colloidal mixture was continued under stirring conditions for 2 hours. To collect the synthesized nanoparticles, centrifugation at 4000 rpm for 15 minutes was performed, then the prepared nanoparticles were washed three times with ultrapure water and dried in an oven at 100 °C in air.

Characterization of PBA $Cu_3[Co(CN)_6]_2$

X-ray photoelectron spectroscopy (XPS) analysis using a Thermo Fisher Scientific ESCALAB (USA) was performed for studying the chemical composition of PBA. Raman spectroscopy was recorded on the prepared sample to determine their chemical content and molecular structure using a Witec Alpha 300 RA confocal Raman microscope with laser excitation at 532 nm. For function group analysis, Fourier transform infrared (FTIR) spectra were recorded using a Vertex 80V FTIR spectrometer (Bruker, Germany). The crystal structure was studied by X-ray diffraction (XRD) using a PANalytical X'Pert diffractometer (Malvern, UK). The measurements were performed using CuKα1 radiation at 45 kV and 40 mA. The surface morphology was characterized using Quattro S scanning electron microscope (SEM) (Thermo Fisher Scientific, USA). The N_2 adsorption–desorption isotherms were determined using the BELsorp

max surface analyzer (BEL Japan Inc, Japan). The specific surface areas were then calculated employing the Brunauer, Emmett, and Teller (BET) theory.

The progress of reduction reaction was tracked by UV-VIS spectrophotometry using a 1601 PC UV-Visible double-beam spectrophotometer (Shimadzu, Japan).

Study of the catalytic activity of PBA toward reduction of MO

For the catalytic reduction of azo dye MO, experiments were conducted in an aqueous medium using $NaBH_4$ as a reducing agent and the synthesized PBA as nanocatalyst. The degradation rate was measured using UV-vis spectrophotometry. In a quartz cuvette, 2.5 mL of BRB pH 9, 100 μL of MO aqueous solution (C = 3 mM), 200 μL of $NaBH_4$ (C = 300 mM) aqueous solution, and 10 μL of an aqueous suspension of PBA (C = 1000 μg mL^{-1}) were added. All experiments were performed at room temperature without stirring. The change in peak intensity of MO at 466 nm was monitored with time. Control experiments were performed using the same steps but in absence of PBA nanocatalyst.

Results and discussion

Characterization of PBA $Cu_3[Co(CN)_6]_2$

Fig. 1a illustrates the typical X-ray diffraction (XRD) patterns obtained for the prepared copper(II) hexacyanocobaltate(III) ($Cu_3[Co(CN)_6]_2$). The diffraction peaks were observed at 2θ angles of 17.82°, 25.24°, 29.66°, 35.87°, 40.09°, 44.30°, 51.52°, 54.93°, 58.14°, 66.96° and 70° corresponding to the indexed crystallographic planes (200), (220), (311), (400), (420), (422), (440), (600), (620), (640), and (642), respectively. The analysis of the indexed patterns revealed that the crystalline structure of $Cu_3[Co(CN)_6]_2$ conforms to a face-centred cubic (FCC) structure, and fits with standard values (JCPDS card no. 002-0169, space group *Fm*3*m*). The XRD analysis was well matched with the reported studies in the literature.[32,33] For the calculation of the average crystallite size (D) of ($Cu_3[Co(CN)_6]_2$), the Scherrer–Debye formula was employed, using the predominant peak observed at 17.82°, corresponding to the (200) plane:

$$D_{(hkl)} = \frac{k\lambda}{\beta_{(hkl)} \cos\theta} \quad (1)$$

where k represents the Debye constant, λ denotes the X-ray wavelength, β indicates the line broadening at full width at half maximum of the diffraction peak, and θ represents the Bragg's angle.[34] Following these calculations, the determined crystallite size of $Cu_3[Co(CN)_6]_2$ was approximately 44 nm.

Raman spectroscopy serves as a valuable tool for evaluating various valence states. Fig. 1b illustrates the Raman spectrum of $Cu_3[Co(CN)_6]_2$, where the peaks detected at 2195 cm^{-1} and 2215 cm^{-1} correspond to the stretching of cyanide ions. The two peaks at frequencies 2195 cm^{-1} and 2215 cm^{-1}, which are merged and prominent on the broad peak, can be attributed to the Co^{3+}–CN–Cu^{2+} interactions. These findings serve as confirmation of the coexistence of mixed valence states within the $Cu_3[Co(CN)_6]_2$ compound.

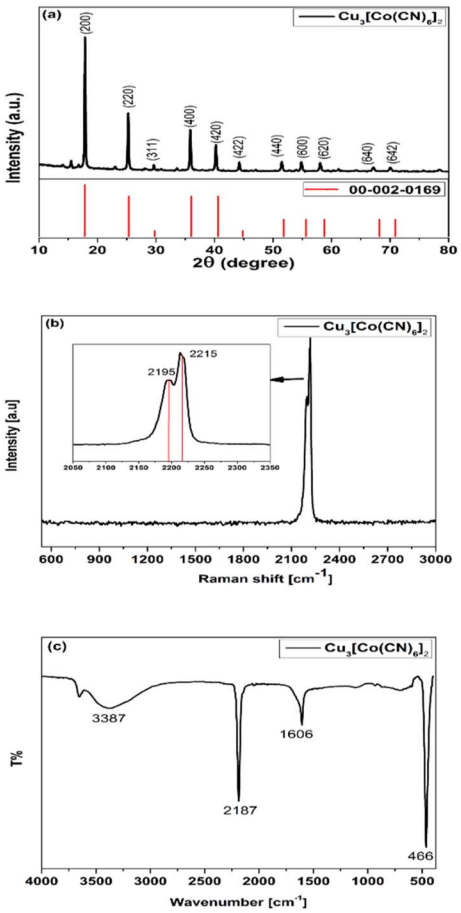

Fig. 1 (a) XRD patterns, (b) Raman spectrum, and (c) FTIR spectrum for $Cu_3[Co(CN)_6]_2$ nanocatalyst.

The information about electronic structure and coordination sites of $Cu_3[Co(CN)_6]_2$ compound can be obtained from the FT-IR analysis, as shown in Fig. 1c. The absorption bands observed in this analysis are associated with the vibrations of –CN, Co–C, and water. The broad absorption band observed from 3300 to 3470 cm^{-1}, was attributed to the stretching mode of H_2O (ν(O–H)) and 1604 cm^{-1} attributed to bending vibrations mode. This characteristic is commonly associated with presence and uncoordinated water molecules.[35] Normally, the main peak appears as a sharp band, but in this case, it was broadened due to the movement of hydrogen-bonded water, as inferred from the FT-IR analysis that water molecules peaks were obviously observed. Additionally, the main peak of the prepared $Cu_3[Co(CN)_6]_2$ is observed at a position of 466 cm^{-1}. The most of $M_x[Co(CN)_6]_2$ compounds exhibit a vibration in the range of 430–470 cm^{-1}, representing a sharp peak that provides information about the Co–C bonding in $Co(CN)_6$.[32]Furthermore, the stretching frequency at approximately 2187 cm^{-1} provides evidence of the presence of bridging –CN groups between two metal atoms.[36,37] In comparison to other transition metal cobalt cyanides, copper demonstrates a higher stretching frequency, suggesting a strong bond between copper and nitrogen atoms.[33]

X-Ray Photoelectron Spectroscopy (XPS) was used as a sensitive approach for elucidating the surface compositions

and chemical states of pure PBA nanomaterials, and the results of this analysis are shown in Fig. 2. The comprehensive surface survey illustrated in Fig. 2a reveals the existence of all detected elements, namely C, N, Co, and Cu. This observation suggests that the surface exclusively contains the compound $Cu_3[Co(CN)_6]_2$.

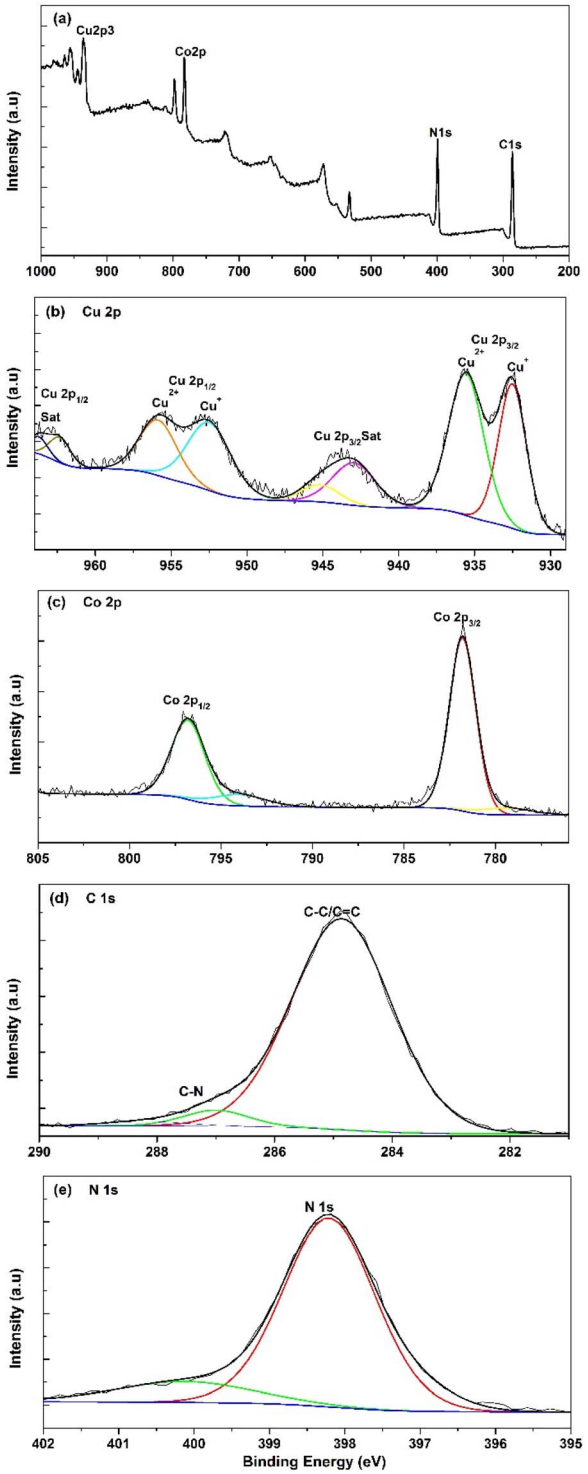

Fig. 2 (a) XPS survey spectrum for $Cu_3[Co(CN)_6]_2$, and its high-resolution XPS spectra of (b) Cu, (c) Co, (d) C, and (e) N.

The deconvolved XPS spectra for the Cu 2p core level are shown in Fig. 2b. The doublet peaks at around 932.52 eV and 935.56 eV in $Cu_3[Co(CN)_6]_2$ are assigned to Cu $2p_{3/2}$, whereas the peaks at 952.47 and 955.56 eV are attributed to Cu $2p_{1/2}$, respectively. Additionally, several satellite peaks at 939.83, 943.72, 962.69, and 963.87 eV are observed for Cu $2p_{3/2}$ and Cu $2p_{1/2}$, confirming the presence of an incompletely filled Cu 3d shell. Furthermore, the fitted peaks at 932.52 eV and 952.4 eV are revealing of Cu^+, whereas the peaks at 934.56 eV and 954.2 eV are associated with Cu^{2+}.[38,39] According to Fig. 2c, the deconvolution of the high-resolution XPS spectrum of Co 2p in $Cu_3[Co(CN)_6]_2$ revealed two spin–orbit peaks with binding energies of 781.8 and 796.8 eV that correspond to Co $2p_{3/2}$ and Co $2p_{1/2}$ with splitting values of 15.8 eV. The gathered data match the previously reported values in the literature. The high-resolution spectrum of C 1s (Fig. 2d.) in the prepared sample exhibits a predominant peak that can be further deconvoluted into two peaks centered at 284.86, and 287 eV, respectively, corresponding to C–C/C=C and C–N bonds respectively.[40] Furthermore, Fig. 2e shows the deconvolution of the high-resolution spectrum of N 1s that revealed a significant peak centered at 398.19 eV, which is attributed to the C–N bonds of the $[Co(CN)_6]^{4-}$ coordinated with Cu.[41] These observations are consistent with the XRD results, confirming the successful synthesis of the $Cu_3[Co(CN)_6]_2$ compound.

The surface morphology of the studied PBA was identified using SEM under different magnifications as represented in Fig. 3. The SEM images of the prepared $Cu_3[Co(CN)_6]_2$ showed nanosized particles with irregular shape. Aggregation of some nanoparticles can be observed which may be attributed to the high surface energy.

Moreover, the surface area of the prepared PBA was assessed *via* BET measurements at −196 °C as shown in Fig. S1 (ESI†).

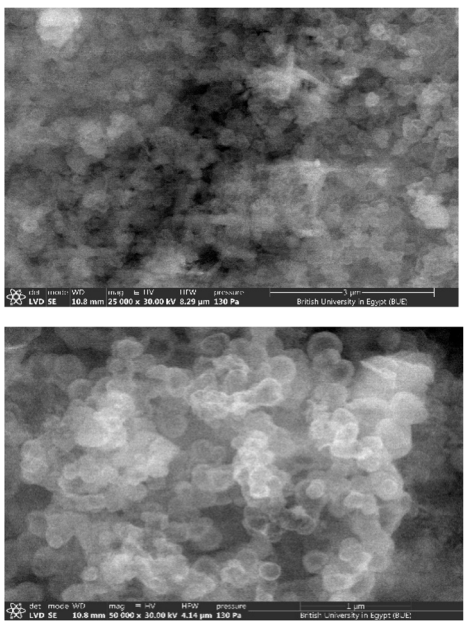

Fig. 3 SEM image for $Cu_3[Co(CN)_6]_2$ nanocatalyst.

The adsorption/desorption isotherm was further plotted as shown in Fig. S2.† The results assured the high surface area for the prepared nanoparticles with specific area 89.18 $m^2\ g^{-1}$.

Catalytic reduction of MO using PBA ($Cu_3[Co(CN)_6]_2$) nanocatalyst

The release of toxic azo dyes as MO in environment from different industries represents public health concern and a serious environmental problem. The azo dye MO is proved to be toxic, carcinogenic, tumorigenic, mutagenic, and genotoxic azo dye. Therefore, conversion of hazardous MO azo dye to less harmful products like 4-aminobenzenesulfonic acid and *N*,*N* dimethylbenzene 1,4 diamine (DMBD) is needed. 4-Aminobenzenesulfonic acid; commonly known as sulfanilic acid is an indirect FDA approved food additive according to the U.S. Code of Federal Regulations (CFR 21). Derivatives of sulfanilic acid are used for treatment of infections caused by Gram-positive and Gram-negative bacteria and some protozoa. DMBD can act as an antioxidant, as it has been shown to inhibit the formation of free radicals.

The catalytic reduction of azo dye MO was conducted using $NaBH_4$ as a reducing agent and the synthesized PBA as nanocatalyst (Fig. 4). The progress of reduction reaction was tracked by UV-VIS spectrophotometry with time. The absorbance at 465 nm in MO spectrum is ascribed to the conjugation originating from the presence of azo bond and dimethylamino electron donating group. After addition of PBA nanoctalyst, the peak intensity of MO at 465 nm decreased rapidly till complete disappearance after 105 s as shown in Fig. 5. On the other hand, a new peak appeared at 250 nm corresponding to hydrazine derivatives.[17] Therefore, the monitored spectra demonstrated the azo bond cleavage and the products formation. The yellow color of MO was completely decolorized in 105 s indicating complete reduction of MO. As a control experiment, the reduction of MO using $NaBH_4$ was investigated in absence of PBA.

As shown in Fig. 6, a very slight decrease in MO peak intensity at 465 was observed after 30 min. Reduction of MO with $NaBH_4$ is thermodynamically feasible. However, the large kinetic barrier between the MO as electron acceptor and $NaBH_4$ as electron donor make the reaction kinetically difficult. Thus, the uncatalyzed reaction is extremely slow. The PBA nanocatalyst facilities the electrons transfer from BH_4^- to MO making the reaction kinetically favorable by decreasing kinetic barrier.[11,12] This demonstrated the powerful catalytic activity of PBA toward reduction of MO. The rate constant (k) of MO reduction was assessed using a pseudo-first-order kinetic model due to presence of $NaBH_4$ in excessive amount relative to MO. Therefore, it was assumed that the rate of reaction was solely dependent on MO concentration. The equation of pseudo-first-order kinetic is represented as $\ln(C_t/C_0) = -kt$. It can also be described as $\ln(A_t/A_0) = -kt$. To monitor the progress in reduction of MO in presence of PBA ($Cu_3[Co(CN)_6]_2$), $\ln(A_t/A_0)$ *versus* the reduction time was plotted and illustrated in Fig. 7.

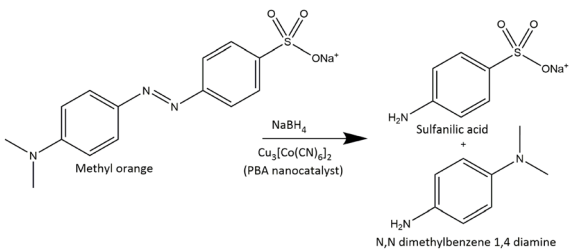

Fig. 4 Reduction of MO by $NaBH_4$ using PBA ($Cu_3[Co(CN)_6]_2$) as nanocatalyst.

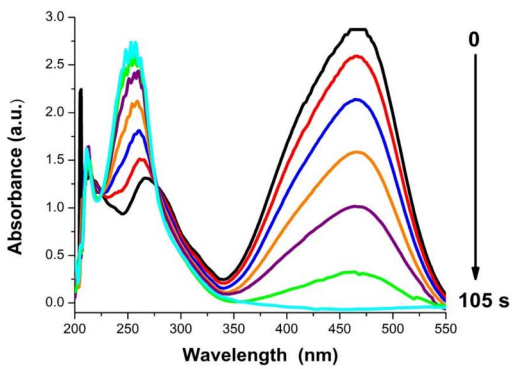

Fig. 5 UV-vis spectra for the reduction of MO by PBA ($Cu_3[Co(CN)_6]_2$) at various time intervals.

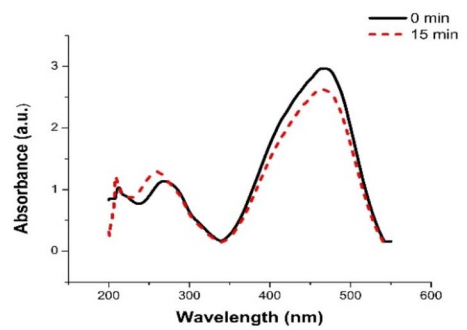

Fig. 6 UV-visible spectra for the reduction of MO without using a catalyst.

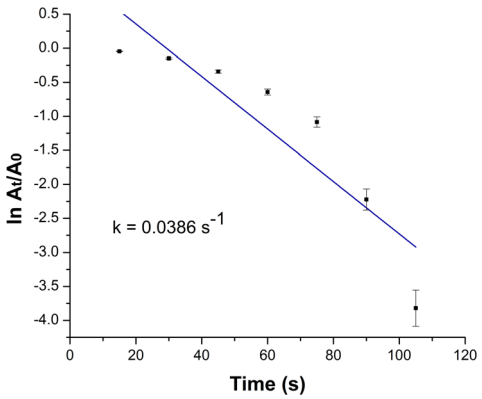

Fig. 7 Kinetics plot of $\ln(A_t/A_0)$ against time for reduction of MO using PBA ($Cu_3[Co(CN)_6]_2$) as nanocatalyst.

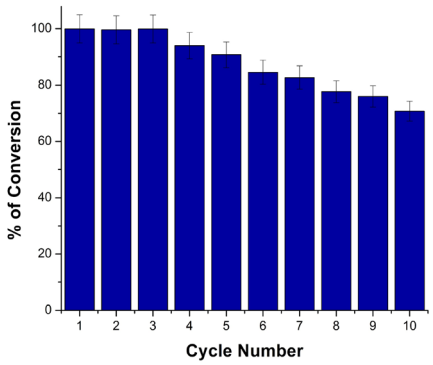

Fig. 8 % of Conversion of MO using PBA ($Cu_3[Co(CN)_6]_2$) as nanocatalyst after ten different cycles.

The apparent rate constant (k) was calculated from the slope of the plot and found to be 0.0386 s^{-1}. Further control experiments were carried out in the dark (keeping all the chemicals covered by aluminium foil) and measuring the samples in the dark. It was found that the catalytic reduction of MO still occurred within 105 s with $K = 0.0349\ S^{-1}$. Moreover, when the nanocatalyst was added to the dye in absence of $NaBH_4$, no degradation of the dye was observed over 5 min as shown in Fig. S3 (ESI†). This indicates that the catalytic process depends mainly on reductive catalysis while photocatalysis doesn't contribute to the complete degradation of MO dye.

Effect of medium pH on catalytic activity of PBA ($Cu_3[Co(CN)_6]_2$) nanocatalyst

The catalytic activity of PBA ($Cu_3[Co(CN)_6]_2$) nanocatalyst toward reduction of MO by NaBH4 was investigated under different pH (acidic; pH 5, neutral; 7 and basic; pH 9). The concentration of nanocatalyst was kept minimum (10 μg) in all experiments. The fastest catalytic reduction rate was obtained in alkaline conditions (pH 9) where k was 0.0386 s^{-1} and the total reduction time was only 105 s. As the pH decreased, the rate slowed down showing k of 0.0134 s^{-1} and 0.001 s^{-1} at pH 7 and 5, respectively. After 105 s, 71.6% of MO was reduced at pH 7, while only 33.0% conversion was achieved at pH 5.

MO is one of the very common water-soluble azo dyes that is broadly used in textile, painting, printing, and paper industries and mostly discharged in industrial wastewater.[42] The effluent generated from these industries is often characterized by alkaline pH.[43–45] Hence, from the obtained results, the powerful catalytic activity of the proposed nanocatalyst in alkaline pH is of a great advantage to eliminate hazardous MO azo dye in alkaline industrial wastewater. Biological treatment of textile effluent is often restricted due to the alkaline pH which affects the growth and metabolism of microbial cells.[46]

Reusability of the synthesized PBA ($Cu_3[Co(CN)_6]_2$) nanocatalyst

Reusability of the catalyst is important to be investigated. A stable catalyst that can be used several times without being deactivated is of economic value as it decreases the cost of the process. To evaluate the reusability and stability of the synthesized PBA nanocatalyst ($Cu_3[Co(CN)_6]_2$), the reduction process was repeated for several cycles using the same catalyst. Without catalyst regeneration, a new batch of MO was added to the reaction mixture each time after finishing the catalytic reduction cycle. The experiments were performed in triplicate. After ten successive catalytic reduction cycles, the proposed PBA catalyst was still able to reduce MO completely with slight increase in the total reduction time (Fig. 8). The ($Cu_3[Co(CN)_6]_2$) retained almost the same powerful catalytic activity after ten reaction cycles demonstrating excellent stability and reusability.

Comparison of the catalytic efficiency of the proposed PBA with the other reported catalysts for reduction of MO

The catalytic performance of the synthesized PBA ($Cu_3[Co(CN)_6]_2$) was compared with the other catalysts reported in the literature for MO reduction as illustrated in Table 1. With using just 10 μg of the proposed nanocatalyst, a higher k was achieved with significant decrease in total time needed for

Table 1 Comparison of the catalytic efficiency of the proposed PBA with the other reported catalysts for reduction of MO

Catalyst	$NaBH_4$ amount	Catalyst amount	k (s^{-1})	Reaction completion time (min)	Ref.
CuAg/ZnO/carbon black-cellulose acetate sheets	0.5 mL (1 M)	0.5 cm^2	1.5×10^{-3}	12	17
Ag nanostructure	25 mL (0.033 M)	1 cm^2	0.56×10^{-3}	60	13
PANI/NiO	N/A	10 000 μg	1.0×10^{-3}	30	18
$NiFe_2O_4/\gamma$-Fe_2O_3	0.5 mL (0.3 M)	100 μg	1.35×10^{-3}	36	19
$CoFe_2O_4/\gamma$-Fe_2O_3	0.5 mL (0.3 M)	100 μg	1.17×10^{-3}	36	
SDS@Ag NPs	0.5 mL (0.025 M)	448 μg mL^{-1}	6.4×10^{-3}	21	14
Pd NPs	1 mL (0.01 M)	4500 μg	$1.36–2.2 \times 10^{-3}$	12–18	15
Cu NPs	0.5 mL (0.2 M)	5000 μg	8.6×10^{-3}	4	16
C@Fe	1 mL (0.5 M)	5000 μg	15.3×10^{-3}	4	20
Ag NPs	0.4 mL (0.1 M)	25–45 μg	14.4×10^{-3}	6	47
Au NPs	0.5 mL (0.6 M)	12.5 μg	8.6×10^{-3}	5	48
PBA ($Cu_3[Co(CN)_6]_2$)	0.2 mL (0.3 M)	10 μg	38.6×10^{-3}	1.75	This work

complete reduction of MO. It can be easily concluded that the proposed PBA has outstanding catalytic activity toward the reduction of MO azo dye compared to the other reported catalysts.

Conclusions

In this work, an eco-friendly PBA nanocatalyst was synthesized *via* facile and low-cost coprecipitation method without using toxic organic solvents. The synthesized PBA showed powerful catalytic activity toward the degradation of hazardous MO azo dye. The total decolorization of MO was completed in 105 s with a rate constant (k) equal to 0.0386 s^{-1}. Furthermore, the nanocatalyst also showed excellent stability and recyclability for ten consecutive cycles, with no significant decrease in the catalytic performance. Therefore, the proposed PBA is a promising stable, cost-effective, and eco-friendly nanocatalyst for the rapid elimination of hazardous azo dyes in industrial effluents.

Author contributions

All authors contributed to the study conception and design. Material synthesis was performed by Dina A. El Mously and Amr M. Mahmoud. Data collection and analysis were performed by Dina A. El Mously, Amr M. Mahmoud, Mohammed M. Goma, and Hend. Z. Yamani. Material characterization was conducted by Mohammed M. Gomaa and Hend Z. Yamani. The first draft of the manuscript was written by Hend. Z. Yamani and Mohammed M. Gomaa. All authors read and approved the final manuscript.

Conflicts of interest

The authors declare that there is no conflict of interest regarding the publication of this article.

Acknowledgements

This research did not receive any specific grant from funding agencies in the public, commercial, or not-for-profit sectors.

References

1 Z. Carmen and S. Daniela, *Textile Organic Dyes-Characteristics, Polluting Effects and Separation/Elimination Procedures from Industrial Effluents-A Critical Overview*, 2012, DOI: 10.5772/32373.
2 K. T. Chung, *J. Environ. Sci. Health C Environ. Carcinog. Ecotoxicol. Rev.*, 2016, **34**, 233–261.
3 R. N. Bharagava and B. Bhimrao, *Textile Industry Wastewater: Environmental and Health Hazards and Treatment Approaches*, 2018.
4 C. R. Holkar, A. J. Jadhav, D. V. Pinjari, N. M. Mahamuni and A. B. Pandit, *J. Environ. Manage.*, 2016, **182**, 351–366.
5 R. Al-Tohamy, S. S. Ali, F. Li, K. M. Okasha, Y. A. G. Mahmoud, T. Elsamahy, H. Jiao, Y. Fu and J. Sun, *Ecotoxicol. Environ. Saf.*, 2022, 231.
6 K. L. Yeap, T. T. Teng, B. T. Poh, N. Morad and K. E. Lee, *Chem. Eng. J.*, 2014, **243**, 305–314.
7 G. M. D. Ferreira, G. M. D. Ferreira, M. C. Hespanhol, J. de Paula Rezende, A. C. dos Santos Pires, L. V. A. Gurgel and L. H. M. da Silva, *Colloids Surf., A*, 2017, **529**, 531–540.
8 M. M. Hassan and C. M. Carr, *Chemosphere*, 2018, **209**, 201–219.
9 J. Vijayaraghavan, S. J. Sardhar Basha and J. Jegan, *J. Urban Environ. Eng.*, 2013, **7**, 30–47.
10 D. Bhatia, N. R. Sharma, J. Singh and R. S. Kanwar, *Crit. Rev. Environ. Sci. Technol.*, 2017, **47**, 1836–1876.
11 M. M. Khan, J. Lee and M. H. Cho, *J. Ind. Eng. Chem.*, 2014, **20**, 1584–1590.
12 N. Gupta, H. P. Singh and R. K. Sharma, *J. Mol. Catal. A: Chem.*, 2011, **335**, 248–252.
13 M. Sakir and M. S. Onses, *Results Phys.*, 2019, **12**, 1133–1141.
14 K. Naseem, F. Ali, M. H. Tahir, M. Afaq, H. M. Yasir, K. Ahmed, A. m. Aljuwayid and M. A. Habila, *J. Mol. Struct.*, 2022, **1262**, 132996.
15 M. Sahin and I. H. Gubbuk, *React. Kinet., Mech. Catal.*, 2022, **135**, 999–1010.
16 M. Ismail, S. Gul, M. I. Khan, M. A. Khan, A. M. Asiri and S. B. Khan, *Green Process. Synth.*, 2019, **8**, 135–143.
17 S. A. Khan, S. B. Khan, A. Farooq and A. M. Asiri, *Int. J. Biol. Macromol.*, 2019, **130**, 288–299.
18 S. Jamil, Z. Ahmad, M. Ali, S. Rauf Khan, S. Ali, M. Amen Hammami, M. Haroon, T. A. Saleh and M. Ramzan, Saeed Ashraf Janjua, *Chem. Phys. Lett.*, 2021, **776**, 138713.
19 G. M. El-Subruiti, A. S. Eltaweil and S. A. Sallam, *Nano*, 2019, **14**, 1950125.
20 M. A. Ahsan, E. Deemer, O. Fernandez-Delgado, H. Wang, M. L. Curry, A. A. El-Gendy and J. C. Noveron, *Catal. Commun.*, 2019, **130**, 105753.
21 H. Yi, R. Qin, S. Ding, Y. Wang, S. Li, Q. Zhao and F. Pan, *Adv. Funct. Mater.*, 2021, **31**, 2006970.
22 A. A. Karyakin, *Electroanalysis*, 2001, **13**, 813–819.
23 Z. Qin, Y. Li and N. Gu, *Adv. Healthcare Mater.*, 2018, **7**, 1800347.
24 D. Parajuli, A. Takahashi, H. Noguchi, A. Kitajima, H. Tanaka, M. Takasaki, K. Yoshino and T. Kawamoto, *Chem. Eng. J.*, 2016, **283**, 1322–1328.
25 Y. C. López, G. A. Ortega and E. Reguera, *Microporous Mesoporous Mater.*, 2022, **333**, 111755.
26 W.-J. Li, C. Han, G. Cheng, S.-L. Chou, H.-K. Liu and S.-X. Dou, *Small*, 2019, **15**, 1900470.
27 T. Wi-Afedzi, F.-Y. Yeoh, M.-T. Yang, A. C. K. Yip and K.-Y. A. Lin, *Sep. Purif. Technol.*, 2019, **218**, 138–145.
28 F. Matloubi Moghaddam, R. Pourkaveh and M. Ahangarpour, *ChemistrySelect*, 2018, **3**, 2586–2593.
29 Y. Liang, C. Yi, S. Tricard, J. Fang, J. Zhao and W. Shen, *RSC Adv.*, 2015, **5**, 17993–17999.
30 J. Guo, H. Li, D. Wang, L. Zhang, Y. Ma, N. Akram, Y. Zhang and J. Wang, *Catal. Sci. Technol.*, 2018, **8**, 6375–6383.
31 K.-Y. A. Lin, B.-J. Chen and C.-K. Chen, *RSC Adv.*, 2016, **6**, 92923–92933.
32 N. Karikalan, M. Velmurugan, S. M. Chen and K. Chelladurai, *RSC Adv.*, 2016, **6**, 48523–48529.

33 E. J. Canto-Aguilar, M. A. Oliver-Tolentino, G. Ramos-Sánchez and I. González, *Electrochim. Acta*, 2021, **371**, 137828.
34 M. M. Gomaa, M. H. Sayed, M. S. Abdel-Wahed and M. Boshta, *RSC Adv.*, 2022, **12**, 10401–10408.
35 C. L. C. Carvalho, A. T. B. Silva, R. A. S. Luz, G. M. B. Castro, C. da Luz Lima, V. R. Mastelaro, R. R. da Silva, O. N. Oliveira, Jr. and W. Cantanhêde, *ACS Appl. Nano Mater.*, 2018, **1**, 4283–4293.
36 K. Y. A. Lin, B. J. Chen and C. K. Chen, *RSC Adv.*, 2016, **6**, 92923–92933.
37 Q. Qiao, H.-J. Wang, C.-P. Li, X.-Z. Wang and X.-M. Ren, *Inorg. Chem. Front.*, 2021, **8**, 2305–2314.
38 P. Wang, Y. H. Ng and R. Amal, *Nanoscale*, 2013, **5**, 2952–2958.
39 X. Li, W. Kong, X. Qin, F. Qu and L. Lu, *Microchim. Acta*, 2020, **187**, 325.
40 P. r. Bommireddy, M. Kumar, Y.-W. Lee, R. Manne, Y. Suh and S.-H. Park, *J. Power Sources*, 2021, **513**, 230521.
41 H. M. El-Sayed, H. Ezzat Abdellatef, A. M. Mahmoud, H. A. M. Hendawy, O. M. El-Abassy and H. Ibrahim, *Microchem. J.*, 2023, **191**, 108829.
42 A. F. Ali, S. M. Atwa and E. M. El-Giar, in *Water Purification*, Elsevier, 2017, DOI: **10.1016/b978-0-12-804300-4.00006-x**, pp. 209–262.
43 R. M. Jain, K. H. Mody, J. Keshri and B. Jha, *Mar. Pollut. Bull.*, 2014, **84**, 83–89.
44 J. Dasgupta, J. Sikder, S. Chakraborty, S. Curcio and E. Drioli, *J. Environ. Manage.*, 2015, **147**, 55–72.
45 P. K. Majhi, R. Kothari, N. K. Arora, V. C. Pandey and V. V. Tyagi, *Bull. Environ. Contam. Toxicol.*, 2022, **108**, 485–490.
46 A. Bhattacharya, N. Goyal and A. Gupta, *Extremophiles*, 2017, **21**, 479–490.
47 D. Khwannimit, R. Maungchang and P. Rattanakit, *Int. J. Environ. Anal. Chem.*, 2022, **102**, 5247–5263.
48 M. Susan Punnoose, D. Bijimol and B. Mathew, *Environ. Nanotechnol., Monit. Manage.*, 2021, **16**, 100525.